Journal of
Nanoscience and Nanotechnology
Vol. 12, 6359–6367, 2012

RESEARCH ARTICLE

Comparisons Between TiO_2- and SiO_2-Flux Assisted TIG Welding Processes

Kuang-Hung Tseng* and Kuan-Lung Chen

Institute of Materials Engineering, National Pingtung University of Science and Technology, Pingtung 91201, Taiwan

This study investigates the effects of flux compounds on the weld shape, ferrite content, and hardness profile in the tungsten inert gas (TIG) welding of 6 mm-thick austenitic 316 L stainless steel plates, using TiO_2 and SiO_2 powders as the activated fluxes. The metallurgical characterizations of weld metal produced with the oxide powders were evaluated using ferritoscope, optical microscopy, and Vickers microhardness test. Under the same welding parameters, the penetration capability of TIG welding with TiO_2 and SiO_2 fluxes was approximately 240% and 292%, respectively. A plasma column made with SiO_2 flux exhibited greater constriction than that made with TiO_2 flux. In addition, an anode root made with SiO_2 flux exhibited more condensation than that made with TiO_2 flux. Results indicate that energy density of SiO_2-flux assisted TIG welding is higher than that of TiO_2-flux assisted TIG welding.

Keywords: TIG Welding, TiO_2 Powder, SiO_2 Powder, Stainless Steel, Flux Compound.

1. INTRODUCTION

The TIG welding is one of the main arc welding processes, in which the necessary heat for welding is generated by maintaining an arc between a refractory tungsten electrode and the base metal to be welded. The electrode, the arc, and the area surrounding the molten metal are protected from atmospheric contamination by an envelope of inert gas during heating and subsequent cooling. The TIG technique may be operated autogenously, or filler metal may be added by feeding a consumable wire or rod into the established welds. It is most commonly used to weld thin sections of stainless steel and light metals, such as aluminum, magnesium, and titanium alloys. In addition, the TIG technique can be used for all welding positions (such as flat, horizontal, vertical, and overhead), and generally produces a smooth, clean weld. However, these advantages are offset by the limited thickness of the base metal that can be welded in a single-pass operation and by the low productivity of the process. Low productivity results from a combination of the low welding speed and the multipass welding procedure for thick section plates or heavy wall pipe materials.[1–3] Additional costs are incurred through edge preparation and substantially longer welding time because several passes with filler metal are required to fill the groove joints.

Improvements in productivity in TIG welding technology have long been sought in the welding community. This demand has led to a so-called flux assisted TIG (TIG-flux) welding, a modified TIG welding process that uses flux compounds, such as oxide, chloride, or fluoride to overcome the limitations by increasing joint penetration using a single-pass operation without any edge preparation.[3–11] Activated flux is a mixture of inorganic powder suspended in an organic solvent. Researchers at the E.O. Paton Electric Welding Institute of National Academy of Sciences of Ukraine (Kiev) introduced a novel concept using the TIG-flux welding to increase penetration of titanium alloy welds in the 1960s, as reported by Gurevich et al.[12, 13] The TIG-flux technique intensifies the conventional TIG technique for welding to a thickness of 8–12 mm using a single-pass full penetration weld, without edge preparation, instead of using multipass welding procedures. Furthermore, the sensitivity of weld shape to variations in the chemical composition of the base metals can be reduced when using the specific fluxes. The TIG-flux welding, which boosted the productivity of conventional TIG welding, requires further investigation, particularly to enhance its joint penetration.

Composition of the flux compounds plays a critical role in increasing the penetration of the TIG-flux welds. The required flux composition depends on the chemical, mechanical, and thermal behavior of the various base metals to be welded. Several potential mechanisms have been proposed for the increased penetration in the TIG-flux

*Authors to whom correspondence should be addressed.

welds. Activated flux can increase the joint penetration, mainly because the surfactant (surface-active element) in the molten pool switches the surface tension gradient, and consequently reverses the Marangoni convection pattern, resulting in a deep-penetration weld.[14–16] Lucas and Howse indicated that a redistributed current affects the distribution of heat flux in the arc column, the induced Lorentz (electromagnetic) force, and the convective heat transfer in molten pool.[17] Although these issues have not been entirely resolved, the constriction of arc plasma, which is responsible for increasing the current density at the center of the anode root and the arc pressure on the surface of the molten pool, has been proposed as a possible mechanism to explain the improvement in penetration of the TIG-flux welds.[1–3, 10, 11, 18] To clarify this uncertainty, this study used TiO_2 and SiO_2 as the flux powder and investigated a further potential mechanism. In addition, the metallurgical characterizations of weld metal produced with the oxide powders were evaluated using ferritoscope, optical microscopy, and Vickers microhardness test.

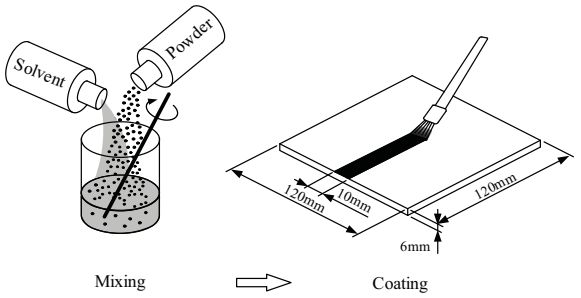

Fig. 1. Schematic diagram of flux preparation.

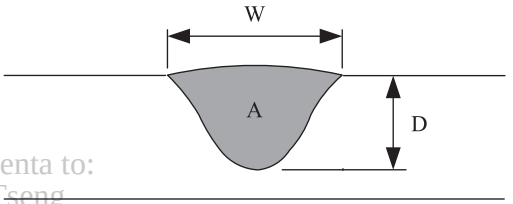

Fig. 2. Schematic representation of weld geometry: D: penetration depth; W: bead width; A: weld cross-sectional area.

2. EXPERIMENTAL DETAILS

The base metals used in this study were wrought austenitic 316 L stainless steel plates; their chemical composition is listed in Table I. The dimensions of the test specimens were 120 × 120 mm with a thickness of 6 mm. The surface of each specimen was roughly grinded with 240 grit (silicon carbide) flexible abrasive paper to remove all impurities, and was subsequently cleaned with acetone prior to welding. The TiO_2 and SiO_2 compounds supplied in powder form were selected as activated flux because their simple composition facilitated the discussion on the manner in which flux increases the penetration of TIG-flux welds. Moreover, TiO_2 and SiO_2 constitute the major composition of several fluxes on the market. Technical information of these powders is shown in Table II. Prior to welding, flux powder was uniformly mixed with methanol to form a paint-like consistency, and was subsequently manually applied with a paintbrush as a sufficiently layer thick to prevent visual observation of the base metal beneath, as shown in Figure 1. In this experiment, the quantity of the flux coating was approximately 4.3 mg/cm^2.

A direct current electrode negative mode was used with a mechanized operation system to allow the welding torch to travel at a constant speed. Single-pass, autogenous TIG welding was performed along the centerline of

Table I. Chemical composition (wt.%, balance Fe) of austenitic 316 L stainless steel.

C	Si	Mn	Cr	Ni	P	S	Mo	N
0.020	0.47	1.77	17.10	10.11	0.031	0.020	2.05	0.048

Table II. Technical information of flux powder.

Flux powder	TiO_2 powder	SiO_2 powder
Origin	Echo Chemical Co., Ltd.	Echo Chemical Co., Ltd.
Molar mass	79.87 g/mol	60.08 g/mol
Density	4.2 g/cm^3	2.6 g/cm^3
Melting point	1,855 °C	1,650 °C
Boiling point	2,972 °C	2,230 °C
Particle size	44 μm	37 μm
Purity	$\geq$ 98%	$\geq$ 99%

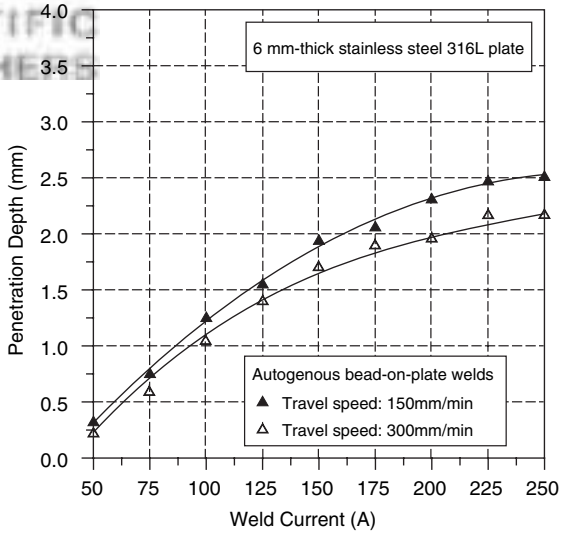

Fig. 3. Effect of weld current and travel speed on penetration depth penetration depth for conventional TIG welding of stainless steel plates.

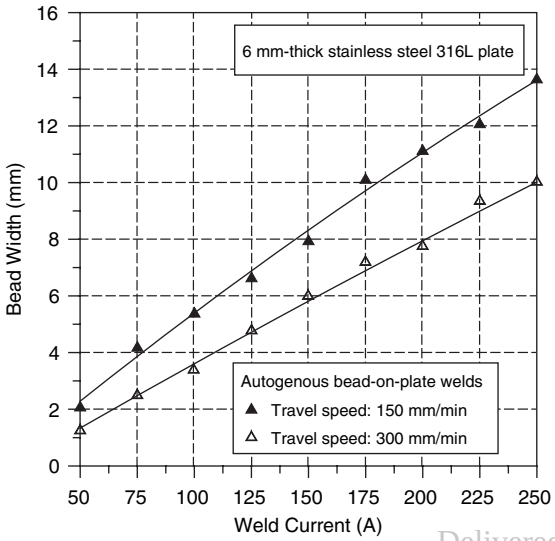

Fig. 4. Effect of weld current and travel speed on bead width for conventional TIG welding of stainless steel plates.

test specimen to produce a bead-on-plate weld. A water-cooled torch with a standard 2% thoriated tungsten electrode was used during the experiments. The electrode rod was 3.2 mm in diameter, with a 45° tip angle and an arc gap of 3 mm. Argon of 99.99% purity, at a constant flow rate of 12 liter/min, was used as the shielding gas. The tip angle of the electrode was grounded, and the arc gap was measured for each new weld prior to welding to ensure that the welding was performed under the same operating conditions. During welding, a charge-coupled device detector system was used to observe and record the images of the arc profile. A digital data acquisition system with a sampling rate of 12 samples per second was also used to continuously measure the current and voltage during the experiments.

Ferrite number (FN) is an arbitrary standardized value designating the ferrite content in austenitic stainless steel weld metal. In this study, FN was measured using a ferritoscope. This device detects phases such as ferrite according to the magnetic susceptibility, which differs from that of paramagnetic austenite. To minimize measurement errors resulting from inhomogeneity in the weld metals, the

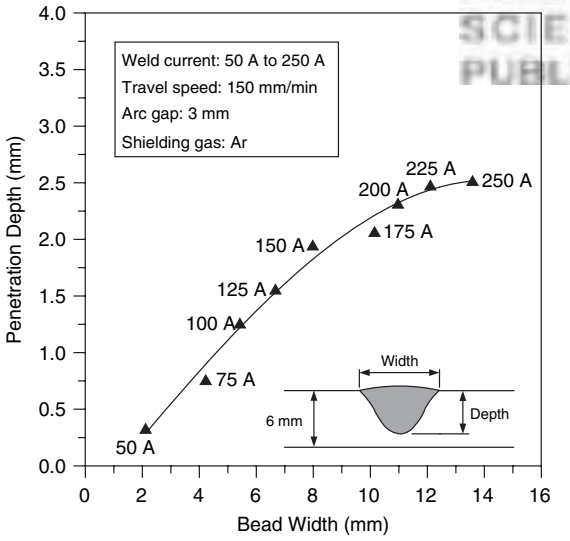

Fig. 5. Comparison of penetration depth correlated to bead width for conventional TIG welding of stainless steel plates.

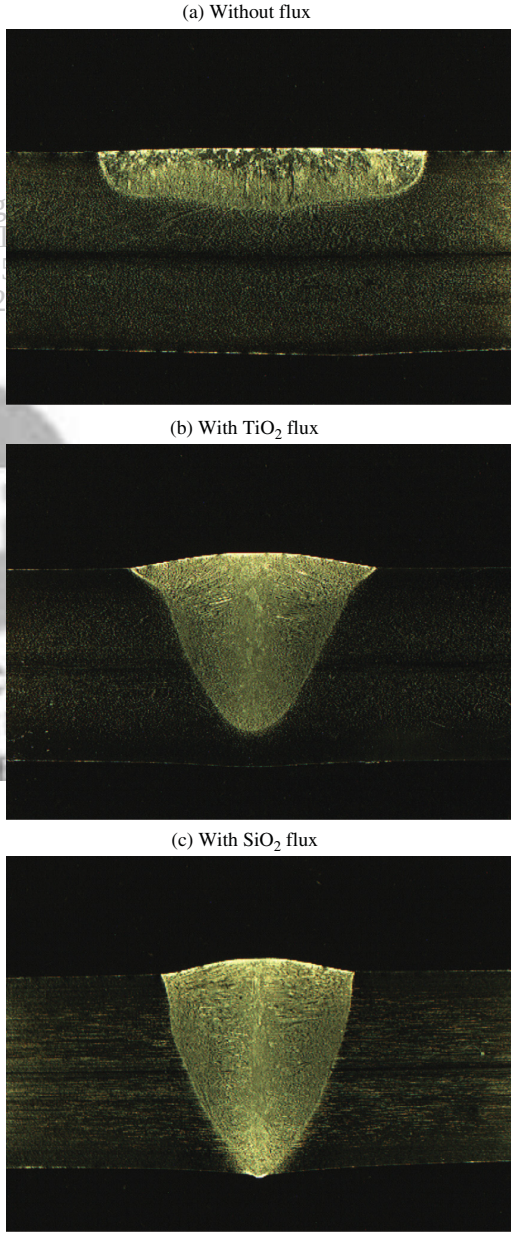

Fig. 6. Cross-sectional macrograph of TIG welds produced with and without flux.

RESEARCH ARTICLE

average value of seven measurements from various locations along the as-welded surface was calculated.

Vickers microhardness test was used to examine the changes in the structure of the welds. The hardness profiles across the weld metal (WM), heat-affected zone (HAZ), and base metal (BM) were measured under a load of 2.94 N for 15 s.

After welding, the surface appearance and geometric shape of the welds were photographed with a stereomicroscope. The geometric shape of the welds was characterized using three quality parameters, that is, penetration depth, bead width, and weld cross-sectional area, as shown in Figure 2. The transverse sections were made at various locations along the welds, whereas samples for metallographic examination were prepared using standard procedures, including mounting, grinding, and polishing to a 0.3 μm finish, followed by electrolytic etching in an electrolyte solution consisting of 10 g oxalic acid and 100 mL water. Each sample was examined with a toolmaker's microscope to measure the depth, width, and area of the welds. Each data point represents the average of three samples. The microstructural characterization of the welds was evaluated using an optical microscopy. An X-ray diffractometer with CuKa source was used to identify the crystalline phases present in the welds. Furthermore, the diffraction results were used to verify the microstructural observation.

3. RESULTS AND DISCUSSION

3.1. Weld Shape of Conventional TIG Welding

Geometric shape is a critical quality characteristic of the welds. The weld current and travel speed are the process parameters of TIG welding that are primarily used to determine the weld shape. Figure 3 shows the variation in penetration depth of autogenous TIG bead-on-plate welds as a function of weld current. Penetration depth is inversely proportional to travel speed at a particular weld current. The measured depth of penetration increased in conjunction with the weld current up to 225 A, beyond which the penetration depth of the welds assumed a constant value of approximately 2.48 mm. In other words, the highest penetration in autogenous TIG welding of stainless steel plate with a thickness of 6 mm that is achievable in a single-pass without edge preparation was limited to 2.5 mm.

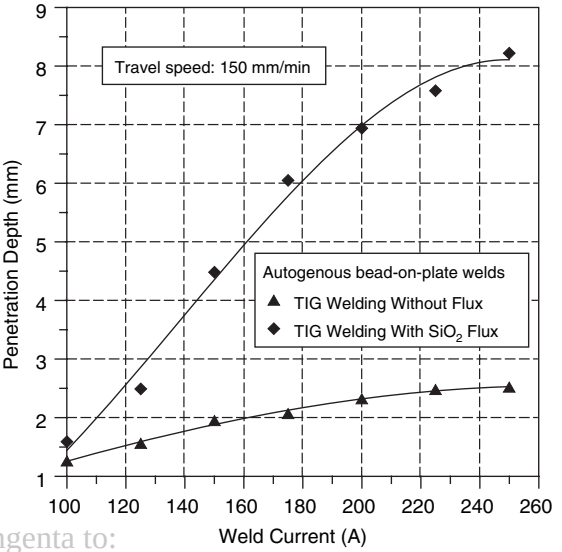

Fig. 8. Effect of weld current on penetration depth of TIG welds produced with and without SiO_2 flux.

Figure 4 shows the variation in bead width of autogenous TIG bead-on-plate welds as a function of weld current. A linear increase in bead width in conjunction with weld current was observed. For a specified TIG welding current, travel speed was inversely related to bead width.

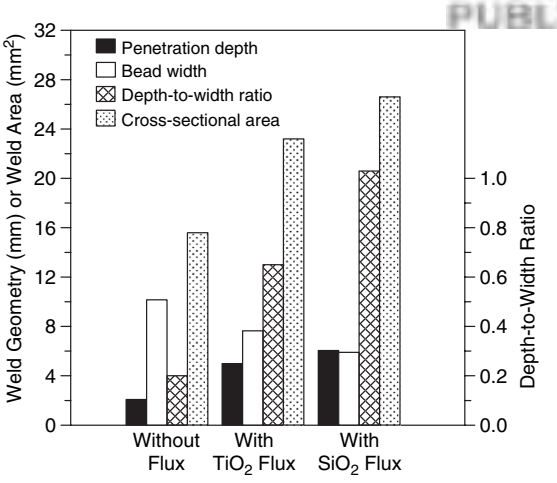

Fig. 7. Geometric characteristic of TIG welds produced with and without flux.

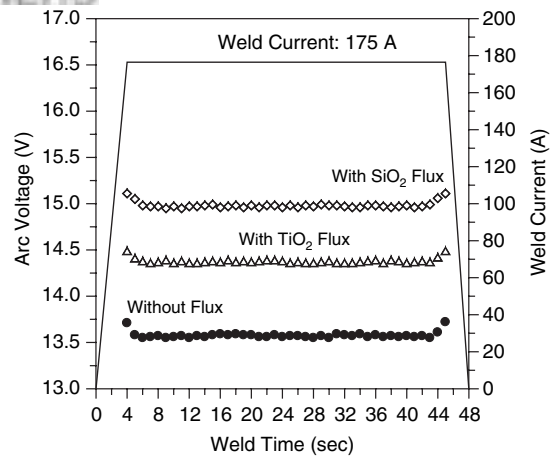

Fig. 9. Weld current and arc voltage of TIG welding made with and without flux.

Figure 5 shows the manner in which penetration depth is related to bead width in the conventional TIG welding of stainless steel plates. The penetration depth increased from 0.33 mm to 2.52 mm, a gain of 2.19 mm, when the weld current increased from 50 A to 250 A, whereas the bead width increased from 2.11 mm to 13.69 mm, an extension of 11.58 mm, when the weld current increased from 50 A to 250 A. The results indicate that by increasing the weld current in an attempt to improve the penetration of conventional TIG welds, the shape of the welds becomes excessively wide with a relatively slight gain in depth.

3.2. Weld Shape of TIG-Flux Welding

In this study, all autogenous bead-on-plate welds were made with 175 A weld current, 150 mm/min travel speed, and 3 mm arc gap. Figure 6 shows the cross-sectional macrograph of TIG welds produced with and without oxide flux in 6 mm-thick stainless steel plates, in which a substantial difference in the weld shape was observed. The TIG welds without flux resulted in a wide, shallow shape (Fig. 6(a)), whereas TIG welds with fluxes exhibited a narrow, deep shape (Figs. 6(b) and (c)). Figure 7 shows the geometric characteristics of TIG welds produced with and without flux. A considerable increase in penetration depth and decrease in bead width occurred when using the TiO_2

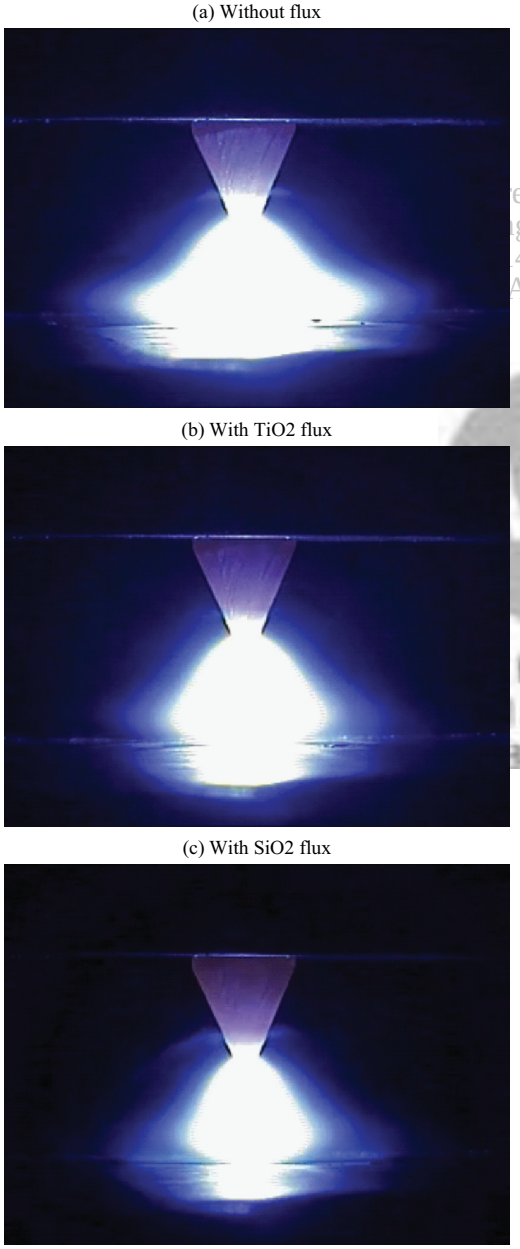

Fig. 10. Plasma column of TIG welding made with and without flux.

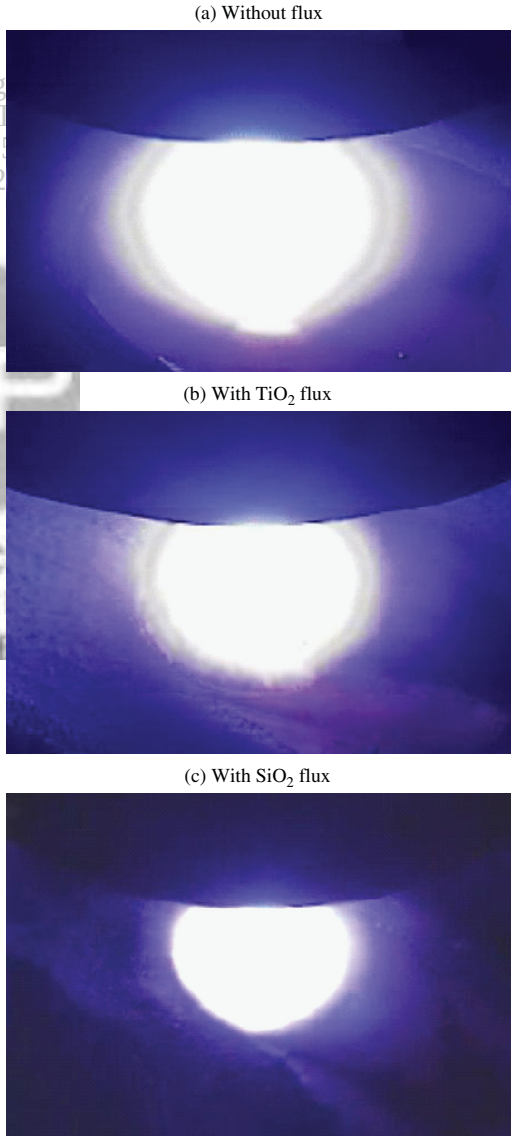

Fig. 11. Anode root of TIG welding made with and without flux.

RESEARCH ARTICLE

and SiO_2 fluxes. In other words, the TiO_2 and SiO_2 fluxes can assist in creating TIG welding with a high depth-to-width ratio in austenitic 316 L stainless steel welds.

A weld with a high depth-to-width ratio is characteristic of an increased energy density of the heat source in welding, which produces an adequate concentration of heat energy. In addition, the energy density is inversely proportional to the duration over which the heat source acts on the weldment. As the energy density of the heat source increases, the overall heat required per unit length of weld deposit decreases. As shown in Figure 8, the depth of penetration that can be achieved in 6 mm-thick stainless steel plate with conventional TIG welding at a high current of 250 A is approximately 2.5 mm. However, full penetration of the welded plate was achieved with the SiO_2-flux assisted TIG welding at a low current of 175 A. The crucial advantage of applying an activated flux to conventional TIG welding is the reduction of arc heat required to achieve a deep-penetration weld.

The efficiency with which the heat source melts the base metal to be welded, that is, the melting efficiency, is of practical interest in arc welding. The melting efficiency of the welds can be determined by measuring its cross-sectional area. The influence of the fluxes on the average cross-sectional area of TIG welds is also shown in Figure 7. With the same welding parameters, the TIG-flux welding can increase the cross-sectional area of the welds. This indicates that TIG-flux welding achieves a higher melting efficiency than conventional TIG welding.

3.3. TiO_2- and SiO_2-Flux Assisted TIG Welding

The TiO_2 and SiO_2 fluxes can increase the penetration of austenitic 316 L stainless steel TIG welds, in which the degree of improvement depends on the composition of the fluxes. Under the same welding parameters, the penetration capability (penetration made with flux relative to the penetration made without flux) of TIG welding made with TiO_2 and SiO_2 fluxes was approximately 240% and 292%, respectively.

With activated fluxes, the charge carriers in a weld arc are redistributed, and the constriction of the plasma column is related to the arc voltage. Figure 9 shows the influence of TIG welding with and without flux on the arc voltage. When the weld current, travel speed, and arc gap were maintained constant, the arc voltage increased when TiO_2 or SiO_2 flux was presented. In TIG welding with TiO_2 or SiO_2 flux, physically constricting the plasma column reduces the conducting cross section of the arc channel; hence, arc voltage must be increased to sustain a continuous arc current at the constant current set by a TIG welding machine. Furthermore, the arc voltage when SiO_2 flux is used is higher than that when TiO_2 flux is used, which may be related to the electronegativity

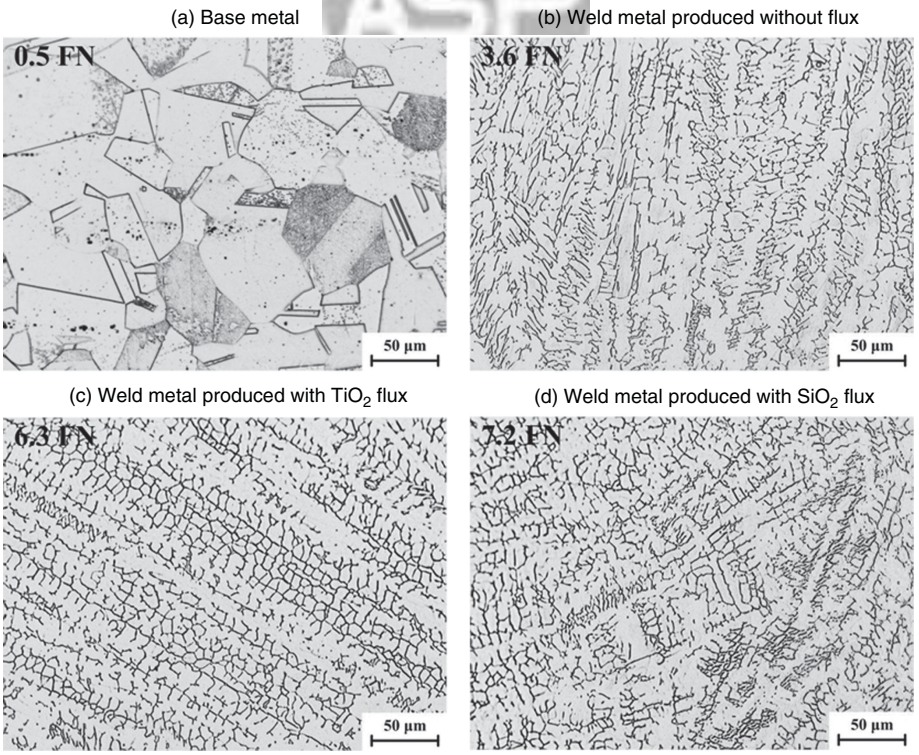

Fig. 12. Microstructure of base metal and TIG welds produced with and without flux.

of the chemical element. With the same oxide structure, expressed as EO_X (where E represents a chemical element), the properties of oxides can be described by the electronegativity of E. Because Si exhibits greater electronegativity than Ti, SiO_2 absorbs more electrons in the outer region of an arc column than TiO_2. Therefore, the plasma column made with SiO_2 flux exhibited greater constriction than that made with TiO_2 flux (Fig. 10).

In addition, because the insulation resistance of SiO_2 flux is higher than that of TiO_2 flux, the anode root on the molten pool surface was more condensed. Such concentration effects of the arc pressure increase the driving forces for the molten metal flow in the weld pool. Therefore, an anode root made with SiO_2 flux exhibited more condensation than that made with TiO_2 flux (Fig. 11).

3.4. Metallurgical Characterizations of TIG-Flux Welds

The microstructure of an austenitic stainless steel matrix consists mainly of full austenite under the slow cooling of equilibrium solidification. However, during the non-equilibrium solidification process, fast cooling usually resulted in the incomplete transformation of ferrite phase to austenite phase. This may occur because the transformation from ferrite phase to austenite phase is a diffusion-controlled process; the fast cooling in the welding process does not offer sufficient time to complete the phase transformation after solidification and cooling to room temperature. This study used an austenitic 316 L stainless steel (ferrite content of 0.5 FN) as a base metal; its microstructure is shown in Figure 12(a). Figures 12(b)–12(d) show the microstructures of the austenitic 316 L stainless steel TIG weld metals. The weld metals exhibited a duplex structure consisting of delta-ferrite dendrites (dark) and equiaxed austenite, and the microstructure of the weld metal differed completely from that of the unaffected base metal. The microstructures of the weld metal produced with and without TiO_2 and SiO_2 flux exhibited a mixed morphology of lacy and skeletal ferrites. The experimental weld metals did not exhibit a considerable difference in solidification structures between TIG welds produced with TiO_2 or SiO_2 flux and those produced without flux. X-ray diffraction (XRD) analysis was used

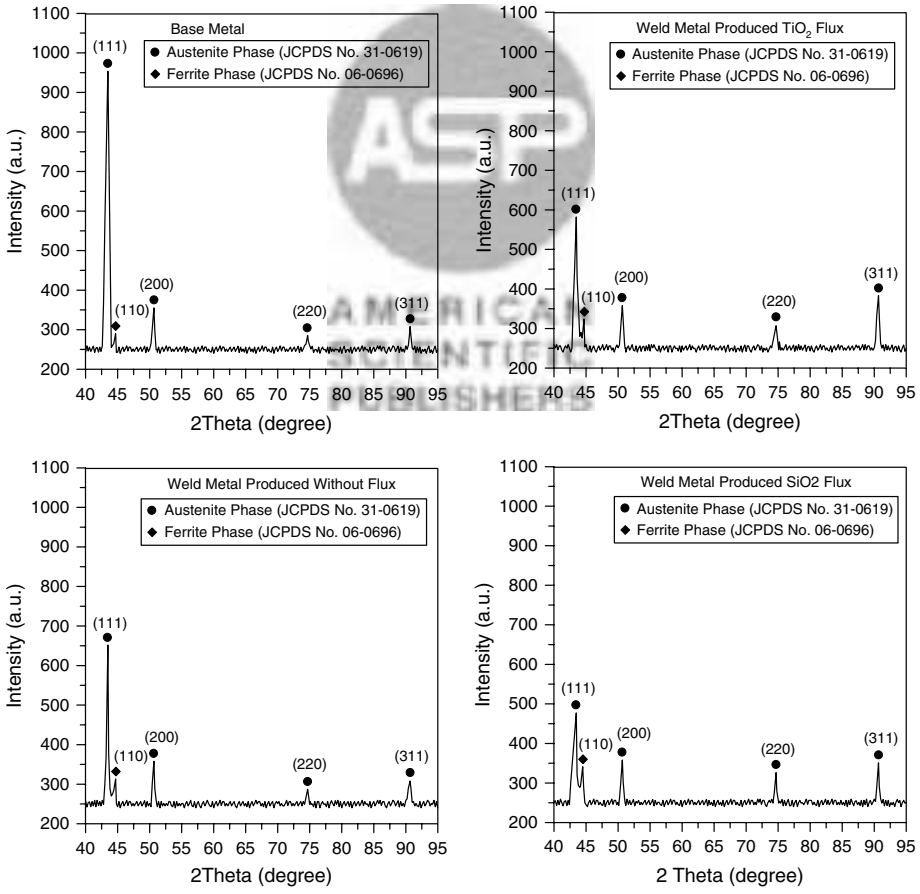

Fig. 13. XRD pattern of base metal and TIG welds produced with and without flux.

RESEARCH ARTICLE

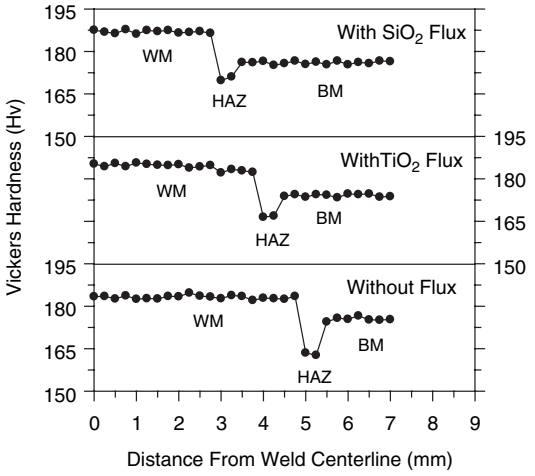

Fig. 14. Hardness profile of TIG weldment produced with and without flux.

to identify and characterize crystalline phases. The XRD result of the base metal and weld metal is provided in Figure 13, which shows that the ferrite and austenite phases were present in all weld metals.

The ferrite content of the weld metals measured using a ferritoscope is also shown in Figure 12. In TIG welding without flux, the measured ferrite content of the weld metals increased to 3.6 FN from its initial value of 0.5 FN. During welding, the fast cooling of the welds caused an incomplete transformation of ferrite phase to austenite phase. Therefore, a large portion of the metastable delta-ferrite structure was unavoidably retained within the austenite matrix. When TiO_2 and SiO_2 fluxes were used, the measured ferrite content in the TIG-flux weld metals increased to 6.3–7.2 FN. This result is closely related to the total heat input used to produce a weld. The most important characteristic of heat input is the manner in which it influences the cooling rate of the welds, thereby affecting the solidification structures of weld metal. The TIG welding with TiO_2 or SiO_2 flux increased the energy density of the heat source, that is, to a low heat input. However, the arc heat of TIG welding without flux has a lower energy density, that is, a high heat input. High heat input resulted in a slow cooling rate and a further transformation from ferrite phase to austenite phase. Consequently, the TIG-flux welding was associated with a low heat input resulting from higher ferrite content than the conventional TIG welding, which corresponds to a high heat input.

In TiO_2- or SiO_2-flux assisted TIG welding, the higher ferrite retained in the austenitic 316 L stainless steel weld metals may be attributed to the fast cooling of the welds instead of the composition of the flux compound, because flux additions act indirectly, and the heat input is the crucial factor affecting the ferrite content retained in the weld metals after solidification.

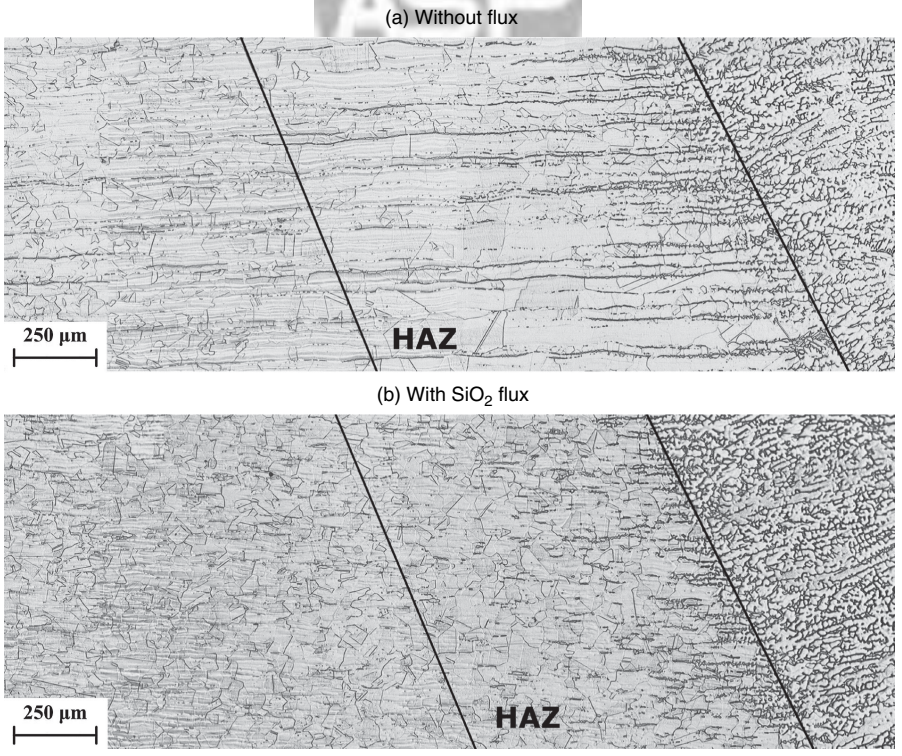

Fig. 15. Metallographic view of microstructure at interface of weld metal and base metal.

3.5. Hardness Profile of TIG-Flux Welds

Figure 14 shows the hardness profile of austenitic 316 L stainless steel TIG weldments produced with and without flux. In a conventional TIG weldment, the average value of the base metal is estimated as 175 Hv, whereas the average values of the weld metal and HAZ are approximately 182 Hv and 163 Hv, respectively. In a TiO_2-flux assisted TIG weldment, the average values of the weld metal and HAZ are approximately 186 Hv and 168 Hv, respectively. In a SiO_2-flux assisted TIG weldment, the average values of the weld metal and HAZ are approximately 188 Hv and 170 Hv, respectively. These results show that the weld metal has the highest hardness, whereas the HAZ has a lower hardness than the base metal. The increase in hardness of the weld metal can be attributed to the presence of the ferrite phase, and the decrease in hardness of the HAZ may be caused by the grain coarsening of the austenite phase.

Figure 15 shows the metallographic view of the microstructure at the interface of the base metal and weld metal produced with and without SiO_2 flux. The base metal is on the left side of each photo, and the weld metal is on the right side of the photos. The HAZ is in the middle, between the base metal and the weld metal. The austenite grain size in the HAZ of the SiO_2-flux assisted TIG welds is clearly smaller than that of the conventional TIG welds. This may have occurred because reducing the heat input increased the solidification velocity, thereby decreasing the grain size of the solidification structure in the TIG-flux welds. In addition, the HAZ range of the SiO_2-flux assisted TIG welds was narrower than that of the conventional TIG welds.

4. CONCLUSIONS

An activated-flux assisted TIG welding of austenitic 316 L stainless steel was studied. The TiO_2 and SiO_2 powders were used as the activated fluxes, and their effects on the weld shape, ferrite content, and hardness profile were investigated. The results are summarized as follows:

(1) The crucial advantage of applying an activated flux to conventional TIG welding is the reduction of arc heat required to achieve a weld with both high depth-to-width ratio and large cross-sectional area.

(2) Under the same welding conditions, the penetration capability of TIG welding with TiO_2 and SiO_2 fluxes was approximately 240% and 292%, respectively. A plasma column made with SiO_2 flux exhibited greater constriction than that made with TiO_2 flux. An anode root made with SiO_2 flux exhibited more condensation than that made with TiO_2 flux.

(3) The experimental weld metals did not show a considerable difference in the solidification structures between the conventional TIG and TIG-flux welds. The microstructures in all weld metals exhibited a mixed morphology of lacy and skeletal ferrites.

(4) An activated-flux assisted TIG welding was demonstrated as a higher energy density arc welding process, and exhibited higher ferrite content in austenitic 316 L stainless steel weld metal than conventional TIG welding. The higher retained ferrite may be attributed to the fast cooling of the welds instead of the composition of the flux compounds.

Acknowledgments: The authors gratefully acknowledge the financial support provided to this study by the National Science Council under the grant no. 100-2221-E-020-012 and the Ministry of Economic Affairs under the grant no. 98-EC-17-A-16-S1-121, Taiwan.

References and Notes

1. H. Y. Huang, S. W. Shyu, K. H. Tseng, and C. P. Chou, *Sci. Technol. Weld. Join.* 10, 566 **(2005)**.
2. H. Y. Huang, S. W. Shyu, K. H. Tseng, and C. P. Chou, *J. Mater. Sci. Technol.* 22, 367 **(2006)**.
3. T. S. Chern, K. H. Tseng, and H. L. Tsai, *Mater. Des.* 32, 255 **(2011)**.
4. M. Tanaka, T. Shimizu, H. Terasaki, M. Ushio, F. Koshi-ishi, and C. L. Yang, *Sci. Technol. Weld. Join.* 5, 397 **(2000)**.
5. M. Marya and G. R. Edwards, *Weld. J.* 81, 291 **(2002)**.
6. A. Rodrigues and A. Loureiro, *Sci. Technol. Weld. Join.* 10, 760 **(2005)**.
7. L. M. Liu, Y. Shen, and Z. D. Zhang, *Sci. Technol. Weld. Join.* 11, 398 **(2006)**.
8. L. M. Liu, Z. D. Zhang, G. Song, and L. Wang, *Metall. Mater. Trans. A* 38, 649 **(2007)**.
9. L. Liu and H. Sun, *Mater. Res. Innovat.* 12, 47 **(2008)**.
10. S. W. Shyu, H. Y. Huang, K. H. Tseng, and C. P. Chou, *J. Mater. Eng. Perform.* 17, 197 **(2008)**.
11. K. H. Tseng and C. Y. Hsu, *J. Mater. Process. Technol.* 211, 503 **(2011)**.
12. S. M. Gurevich, V. N. Zamkov, and N. A. Kushnirenko, *Avtom. Svarka* 9, 1 **(1965)**.
13. S. M. Gurevich and V. M. Zamkov, *Avtom. Svarka* 12, 13 **(1966)**.
14. C. R. Heiple and J. R. Roper, *Weld. J.* 60, 143 **(1981)**.
15. C. R. Heiple and J. R. Roper, *Weld. J.* 61, 97 **(1982)**.
16. C. R. Heiple, J. R. Roper, R. T. Stagner, and R. J. Aden, *Weld. J.* 62, 72 **(1983)**.
17. W. Lucas and D. Howse, *Weld. Met. Fabr.* 64, 11 **(1996)**.
18. D. S. Howse and W. Lucas, *Sci. Technol. Weld. Join.* 5, 189 **(2000)**.

Received: 14 February 2012. Accepted: 21 March 2012.